Journal of Structural Geology, Vol. 14, No. 5, pp. 605 to 620, 1992
Printed in Great Britain

0191-8141/92 $05.00+0.00

The evolution of perpendicular linear fabrics in synkinematically emplaced tourmaline granite (central Moravia–Bohemian Massif)

RADEK MELKA

Institute of Geological Sciences, Charles University Prague, 128 43 Praha 2, Albertov 6, Czechoslovakia

KAREL SCHULMANN

Department of Petrology, Charles University Prague, 128 43 Praha 2, Albertov 6, Czechoslovakia

BARBORA SCHULMANNOVÁ

Geological Survey Prague, Malostranské nám. 19, 118 21 Praha 1, Czechoslovakia

FRANTIŠEK HROUDA

Geofyzika s.p., Ječná 19, 612 46 Brno, Czechoslovakia

and

MICHAL LOBKOWICZ

Geological Survey Prague, Malostranské nám. 19, 118 21 Praha 1, Czechoslovakia

(*Received* 4 *June* 1990; *accepted in revised form* 28 *September* 1991)

Abstract—Sheets of leucocratic peraluminous tourmaline granite were synkinematically emplaced into metasediments of the Svratka Crystalline Unit during the Variscan orogeny. The granite was deformed under high-temperature conditions close to the solidus, as indicated by quartz microstructures and the presence of prism ⟨*c*⟩ glide in quartz. Decrease in the temperature of deformation causing orthogneissification of the granite is documented by transition from prism ⟨*c*⟩ to prism ⟨*a*⟩ and basal ⟨*a*⟩ glide operating in quartz grains.

Two mutually perpendicular stretching lineations originated during high-temperature deformation of the granite. Detailed three-dimensional analysis of tourmaline preferred orientations underlining both lineations has been performed and the distributions have been compared with theoretical predictions of Jeffery and March for rotation of rigid linear markers. The origin of mutually perpendicular linear fabrics is discussed on the basis of numerical models. Transpression, considered as a combination of northwestward shearing accompanied by shortening across and lengthening along the shear plane, is proposed to explain the perpendicular linear fabrics observed.

INTRODUCTION

STRUCTURAL and metamorphic evolution of the Variscan orogen has been interpreted in terms of large-scale nappe emplacement (Suess 1926, Kossmat 1927), connected with lithospheric subduction and collision (Matte 1986, Franke 1989). Stretching and mineral lineations, as well as sense of shear criteria, are used as reliable indicators of direction and sense of crustal-scale movements (Shackleton & Ries 1984).

Stretching lineations are commonly considered to be subparallel to the X-axis of the finite strain ellipsoid (e.g. Nicolas 1984) and consequently subparallel to the principal tectonic movement. However, stretching lineations perpendicular to the expected direction of regional displacement were described in many regions. In addition, two mutually perpendicular stretching lineations exist in some areas (Bouchez *et al.* 1984, Burg *et al.* 1987). Such a geometrical configuration has been explained either in terms of superposed deformations (Cannat & Bouchez 1986) or as a result of combined thrusting and wrenching (Brun *et al.* 1985, Burg *et al.* 1987) or due to complementary conjugate strike-slip movements allowing tectonic escape of overthickened crust (Molnar & Tapponier 1975, Behrmann 1988).

In this paper we discuss the generation of two perpendicular linear fabrics defined by preferred orientation of tourmaline in a sheet-like granitic body. The growth of tourmaline crystals and their preferred orientation are attributed to synkinematic emplacement of this peraluminous granite during the Variscan thrust event.

We will describe the three-dimensional fabric distribution of tourmaline columns associated with two perpendicular stretching lineations lying on commonly oriented foliation planes. These distributions will then be compared with the rotation of rigid linear markers based on the theoretical predictions of Jeffery (1922) and March (1932). Finally, a numerical model of the

fabric evolution will be developed to try to explain the observed patterns in terms of their complex deformational histories.

GEOLOGICAL SETTING

The area studied (*ca* 25 km^2) is situated at the eastern border of the Svratka Crystalline Unit (Fig. 1) which, together with the Moldanubian nappes, occupies a high position in the nappe pile at the eastern margin of the Bohemian massif (Schulmann *et al.* 1991). The Svratka Crystalline Unit and the Moldanubicum contain relics of high-pressure rocks, and were emplaced over lower Moravian nappes, characterized by intermediate pressure and temperature mineral assemblages, during early Variscan convergence dated at around 350 Ma (Van Breemen *et al.* 1982, Matte 1986). An E-vergent sense of nappe emplacement, originally proposed by Suess (1912, 1926) and still supported by some authors (Jaroš & Mísař 1986, Jaroš 1989) is a subject of recent debate. New investigations brought evidence for clear northward or northwestward nappe transport in this area (Schulmann *et al.* 1991).

The Svratka Unit in the area studied (Fig. 1) consists essentially of garnet–mica schist, migmatized two-mica schist and anatectonic peraluminous orthogneiss, rich in tourmaline (Němec 1979). Intercalations of marble, amphibolite and quartzite are present together with some skarns and slices of serpentinite (Weiss 1966). An extensive anatexis developed under amphibolite facies conditions, characterized by the mineral assemblage: quartz + plagioclase + biotite + muscovite + garnet (almandine) ± K-feldspar ± kyanite ± sillimanite.

According to Pertoldová (1986), using different geothermometers and geobarometers (garnet–biotite, garnet–phengite, garnet–plagioclase–quartz–Al_2SiO_5, K-feldspar–plagioclase), the temperature in the garnet–mica schists reached 600–675°C for a pressure estimated at 6–9 kb. Significantly lower temperatures of 550–600°C

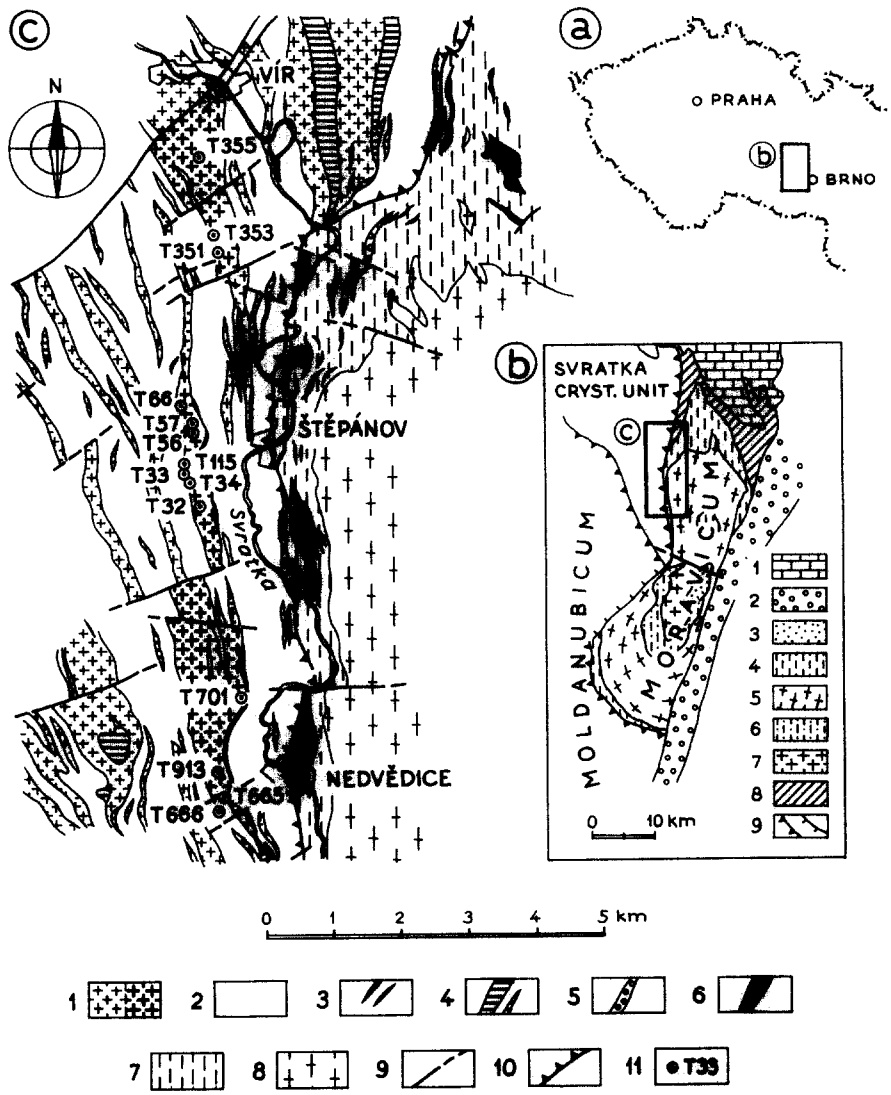

Fig. 1. (a) Geological map of the area under study (after Mísař 1965, Schulmannová 1987). Legend to inset (b): 1—Cretaceous, 2—Permian, 3—Devonian, 4—Outer phyllites, 5—Bíteš orthogneiss, 6—Inner phyllites, 7—Tišnov granitoids, 8—Letovice ophiolitic complex, 9—thrust–fault boundary. Legend to inset (c): 1–4 Svratka crystalline unit: 1—peraluminous orthogneiss without/with tourmaline, 2—mica schist, 3—marble, 4—skarn; 5–8 Moravicum: 5—quartzite, 6—marble, 7—phyllites, 8—Bíteš orthogneiss; 9—fault, 10—thrust, 11—sites of tourmaline analyses.

obtained in peraluminous granite rich in tourmaline are, according to Pertoldová (1986), probably due to the high concentration of boron and fluorine. Growth of muscovite and sillimanite at the expense of kyanite and biotite in the mica schist is associated with retrogression under lower pressure conditions.

MESOSCOPIC STRUCTURES

Foliation and lineations

The regional metamorphic S_1 W-dipping foliation (Fig. 2) is marked by alternation of mica-rich and quartzofeldspathic layers in garnet–mica schist, and by flattened quartz grains and arrangement of micas and feldspar in peraluminous granite. This foliation bears two mutually perpendicular mineral lineations: L_i plunging to the southwest at shallow angles and L_{ii} plunging to the northwest (Fig. 2). Both lineations occur in tourmaline granite as well as surrounding mica schist. In the mica schist these lineations are marked by the alignment of micas, by pressure shadows around garnet porphyroblasts and by elongated quartz lenses. In the granite oriented tourmaline columns up to 20 mm long and elongated quartz and feldspar grains define the lineations.

L_i and L_{ii} never occur together on a single foliation plane so that their mutual relationships cannot be directly observed. Rather they occur in alternating domains several metres thick, the L_{ii} being more common mainly in the northern part of the area studied (Fig. 2). Microstructural evidence indicates that both the L_i and L_{ii} lineations are connected with subsolidus deformation in the leucocratic granite and the L_{ii} lineation exhibits superposition of solid-state flow on early subsolidus stage (see below). The relative ages of L_i and L_{ii} in the first subsolidus stage are not known, that is why we prefer to refer to these lineations as L_i, L_{ii} rather than L_1, L_2.

The sense of shear criteria, e.g. garnets with spiral-shaped inclusion trails in their cores, numerous shear bands and asymmetrical pressure shadows around rotated garnets and feldspars, are connected with L_{ii}

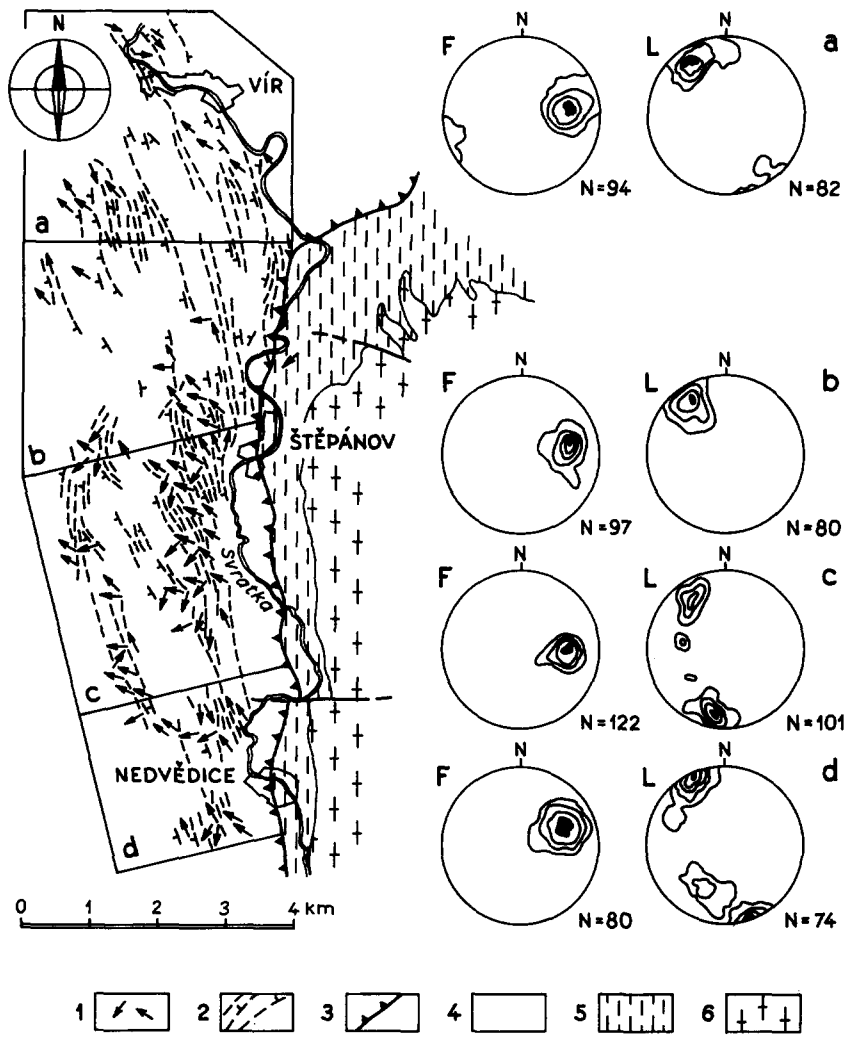

Fig. 2. Structural map of the area studied: 1—mineral and stretching lineations, 2—metamorphic foliation, 3—thrust, 4—mica schists and syntectonic granites of the Svratka crystalline unit, 5—outer phyllites of Moravicum, 6—Bíteš orthogneiss. Orientation diagrams: F—poles to foliation planes, *L*—stretching lineations. Lower-hemisphere, equal-area projection, contours 1, 3, 7, 18 and 24 multiples of uniform distribution. Diagrams a, b, c and d correspond to subareas indicated in the map.

lineation only. These criteria indicate NW-oriented shearing extending throughout metamorphic retrogressive conditions.

The latest stage of granite deformation is represented by planar shear zones with shear planes at a high angle to regional foliation and direction of shear subparallel to the L_{ii} lineation.

Folding

Two phases of folding can be observed in the area.

(1) Rootless F_1 folds several centimetres in size, locally developed in the mica schist, emphasize the composite character of the S_1 metamorphic foliation. It was not possible to measure the orientation of the axes of these folds in the field, so the relationships to both L_i and L_{ii} lineations are impossible to establish.

(2) Cylindrical asymmetric F_2 folds up to 1 m in size refold the S_1 foliation and veins of leucocratic material penetrating into the mica schist. The F_2 folds can be subdivided into two groups according to spatial relations of their axes with the L_i and L_{ii} lineations. The axes of the F_{2i} folds are parallel to the L_i lineation (Fig. 3a) and these folds occur locally in the southern part of the studied area. Northwest-plunging F_{2ii} folds with their axes subparallel to the L_{ii} lineation (Fig. 3a) are more common. Most of the F_{2ii} folds are SW vergent.

The F_{2i} folds are close to tight with axial planes subparallel to S_1 foliation while the F_{2ii} folds are very heterogeneous in style and geometry ranging from open buckle folds with variable axial-plane orientation to tight flattened folds with axial planes subparallel to the S_1 foliation (Fig. 3b). The origin of the F_2 folds, with axes parallel to stretching lineation, may be explained by foliation-parallel extension in the lineation direction. With ongoing deformation the folds were further flattened and their axial planes were reoriented parallel to foliation (Fig. 3b).

QUARTZ MICROFABRIC

Three stages of quartz deformation have been recognized:

(1) deformation of anatectic granite near the solidus conditions which is connected with the origin of both L_i and L_{ii} lineations;

(2) post-solidus deformation of granite associated with the L_{ii} lineation;

(3) low-temperature deformation in heterogeneous shear zones with movement direction subparallel to the L_{ii} lineation.

Quartz microfabric in anatectic granite

Quartz usually occurs as large isolated grains 1–2 mm in size which are slightly elongate in the stretching direction. Grain boundaries are either slightly curved or reveal strongly lobate shapes, suggesting extensive grain boundary migration (Figs. 4a & b). Rectangular mosaic-like grain boundaries (Fig. 4b) indicate a high mobility of grain boundaries controlled by crystallographic orientation (Gapais & Barbarin 1986) at high-temperature conditions. Prismatic subgrain boundaries, commonly transecting the whole grains, are subparallel to the grain elongation, whilst basal or sub-basal subgrain boundaries are ill-defined and form rectangular subgrains with planar prismatic walls (Fig. 4a). Systematic measurements using the U-stage reveal about 70% of prismatic subgrain boundaries and about 20% of basal ones (Fig. 5a).

Quartz *c*-axes show small-circle distribution around the *X*-axis of the finite strain ellipsoid with maxima near L_i and L_{ii} stretching directions. These circles are connected by weaker small circles centred around the *Z*-axis (Figs. 6a & b). These quartz *c*-axis fabrics may be compared with numerically modelled *c*-axis patterns for plane strain deformation of both hexagonal and trigonal

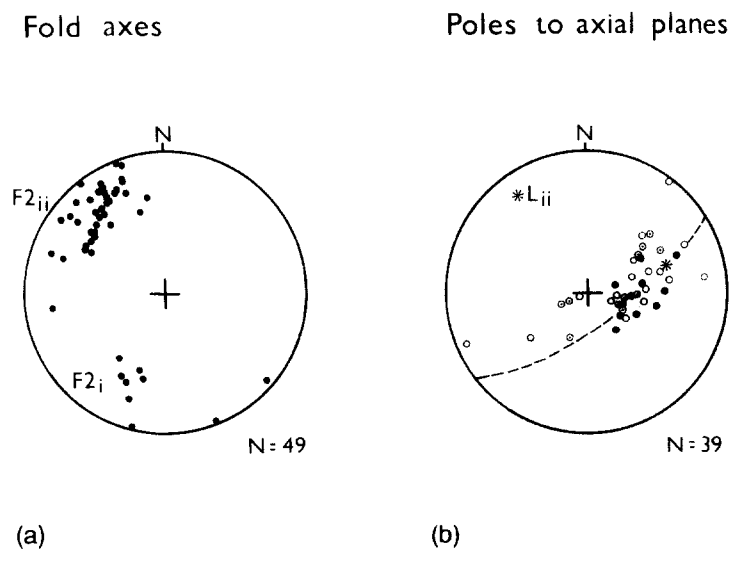

Fig. 3. Folds F_2 refolding the S_1 foliation. (a) Orientation of axes of F_{2i} and F_{2ii} folds parallel with L_i and L_{ii} lineations, respectively. (b) Poles to axial planes of F_2 folds. Open circles = folds with interlimb angle (ILA) > 45°; dotted circles = 45° > ILA > 30°, full circles = ILA < 30°.

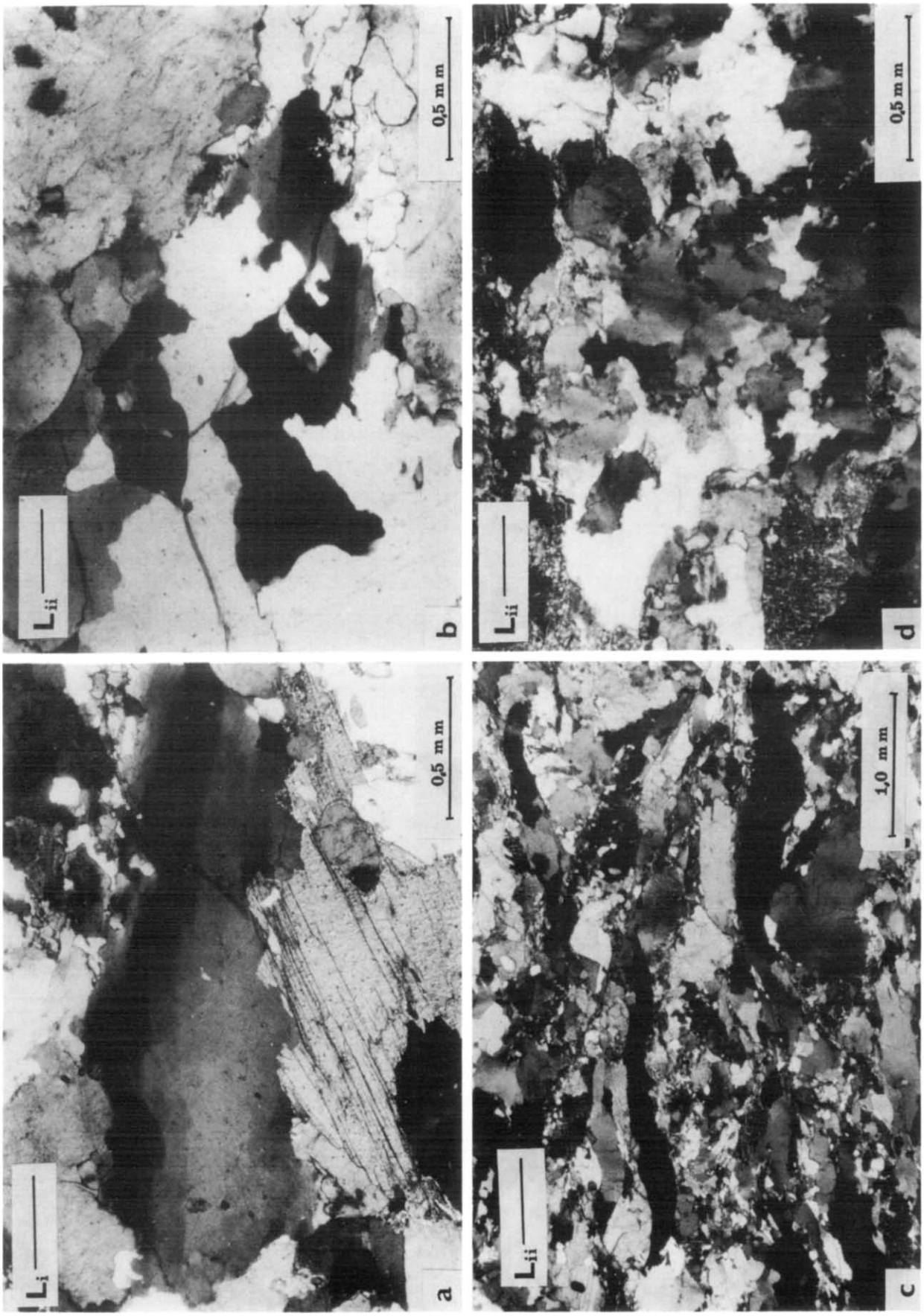

Fig. 4. Quartz microstructures associated with L_i and L_{ii} lineations in the peraluminous granite. All sections are cut parallel to stretching lineation and perpendicular to foliation. (a) Microstructure of anatectic granite with L_i lineations showing large quartz grain with *c*-axis orientation close to L_i. Note the prismatic subgrain boundaries (SGB) cross-cutting the whole grain and perpendicular basal SGB. (b) Microstructure of anatectic granite with L_{ii} lineation. Quartz grains have rectangular mosaic-like grain boundaries and prismatic SGB. *c*-axis is close to L_{ii}. (c) Microstructure of orthogneissified granite with L_{ii} lineation. Quartz forms ribbons with *c*-axis close to the *Y*-axis of the finite strain ellipsoid. (d) Quartz from late shear zone. Strongly recrystallized ribbons with prismatic SGB perpendicular to L_{ii} lineation. *c*-axes are subparallel to foliation pole.

quartz with dominant prism ⟨c⟩ glide (Lister 1981, figs. 2 and 3). Similar natural *c*-axis patterns from granites and migmatites deformed at very high temperature conditions are also reported by Blumenfeld *et al.* (1986) and Gapais & Barbarin (1986). The size of individual quartz grains depends on the orientation of its *c*-axis. Those grains with the *c*-axis close to the principal stretching direction are larger than grains with *c*-axes at a high angle to the *X*-axis (Fig. 5b). The quartz microfabric in anatectic granite can be interpreted in terms of combined prism ⟨c⟩ glide and extensive grain boundary migration in grains oriented favourably for easy prism ⟨c⟩ slip.

Quartz in orthogneissified granite

Quartz forms mono- or poly-crystalline ribbons with straight boundaries between individual grains (Fig. 4c). Prismatic subgrain boundaries transecting the whole grains are generally subparallel to the foliation trace. Quartz *c*-axis fabrics form typical type II crossed-girdle patterns of Lister (1977), with strong maxima parallel to the *Y*-axis of the finite strain ellipsoid (Fig. 6). The quartz deformation occurred in the field of crystal plasticity dominated by prism ⟨a⟩ glide; some minor grain boundary migration is still present.

Quartz in late shear zones

Quartz is present in the form of strongly recrystallized ribbons with irregular boundaries between individual grains. Common internal microstructures are strong undulatory extinction and the presence of numerous prismatic subgrain walls perpendicular to the foliation trace (Fig. 4d). Quartz *c*-axis patterns show intense maxima parallel to the *Z*-axis of the finite strain ellipsoid (Fig. 6). The deformational mode is mainly basal ⟨a⟩ glide accommodated by rotational recrystallization.

TOURMALINE FABRIC ANALYSIS

Tourmaline in peraluminous orthogneiss occurs in the form of euhedral crystals up to 20 mm in size exhibiting variable degrees of preferred orientation. Tourmalines are either dispersed throughout the rock, indicating a magmatic origin, or lie in foliation planes, suggesting later mimetic growth (Němec 1979). Only euhedral magmatic crystals are considered in this study.

The orientation of the long axes of the tourmalines as well as their length and width, have been measured at 14 sites in a N–S-trending body of peraluminous granite (Fig. 1). On average 80 measurements have been made at each locality. Orientations of the tourmaline long axes were plotted on equal-area, lower-hemisphere projections (Fig. 7a). The orientation tensor (Fara & Scheidegger 1963, Scheidegger 1965, Watson 1965, Woodcock 1977, Cobbold & Gapais 1979) was calculated from these data and consequently the eigenvalues E_1, E_2 and E_3 and corresponding eigenvectors $\mathbf{v}_1$, $\mathbf{v}_2$, $\mathbf{v}_3$ determined (Fig. 7b). The ratios of ln (E_1/E_2) and ln (E_2/E_3) were plotted according to Woodcock (1977) (Fig. 7a). Symmetry of the fabric ellipsoid is represented by the *K* value:

$$K = \ln (E_1/E_2)/\ln (E_2/E_3) \quad (1)$$

and the intensity of the preferred orientation is given by the *I* parameter (Lisle 1985):

$$I = 15/2 \times \sum_{i=1}^{3} (E_i - 1/3)^2. \quad (2)$$

I ranges between 0 (no preferred orientation) and 5 (all fabric elements perfectly parallel one to another). In view of the trigonal symmetry, elongated habit and large ductility contrast between markers and matrix, the tourmaline columns may be considered as axial markers (Fernandez 1984). The length/width ratios (*r*) varies from 1.5 to 15, with distributions of *r* varying slightly from site to site (Fig. 8).

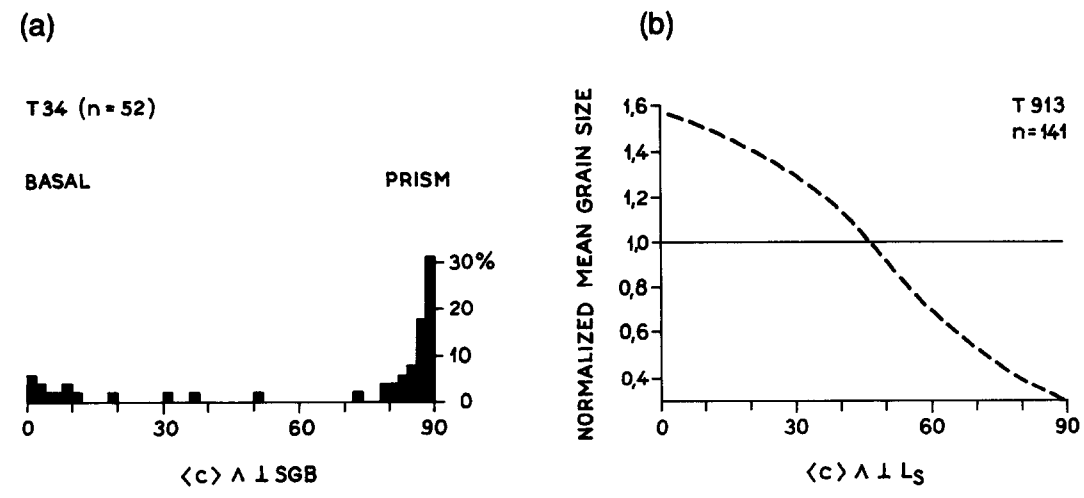

Fig. 5. (a) Distribution of angles between *c*-axes and poles to subgrain boundaries in the anatectic granite. (b) Dependance of the size of quartz grains on their *c*-axis orientation in the anatectic granite. Abscissa—angle between *c*-axis and L_{ii} stretching lineation.

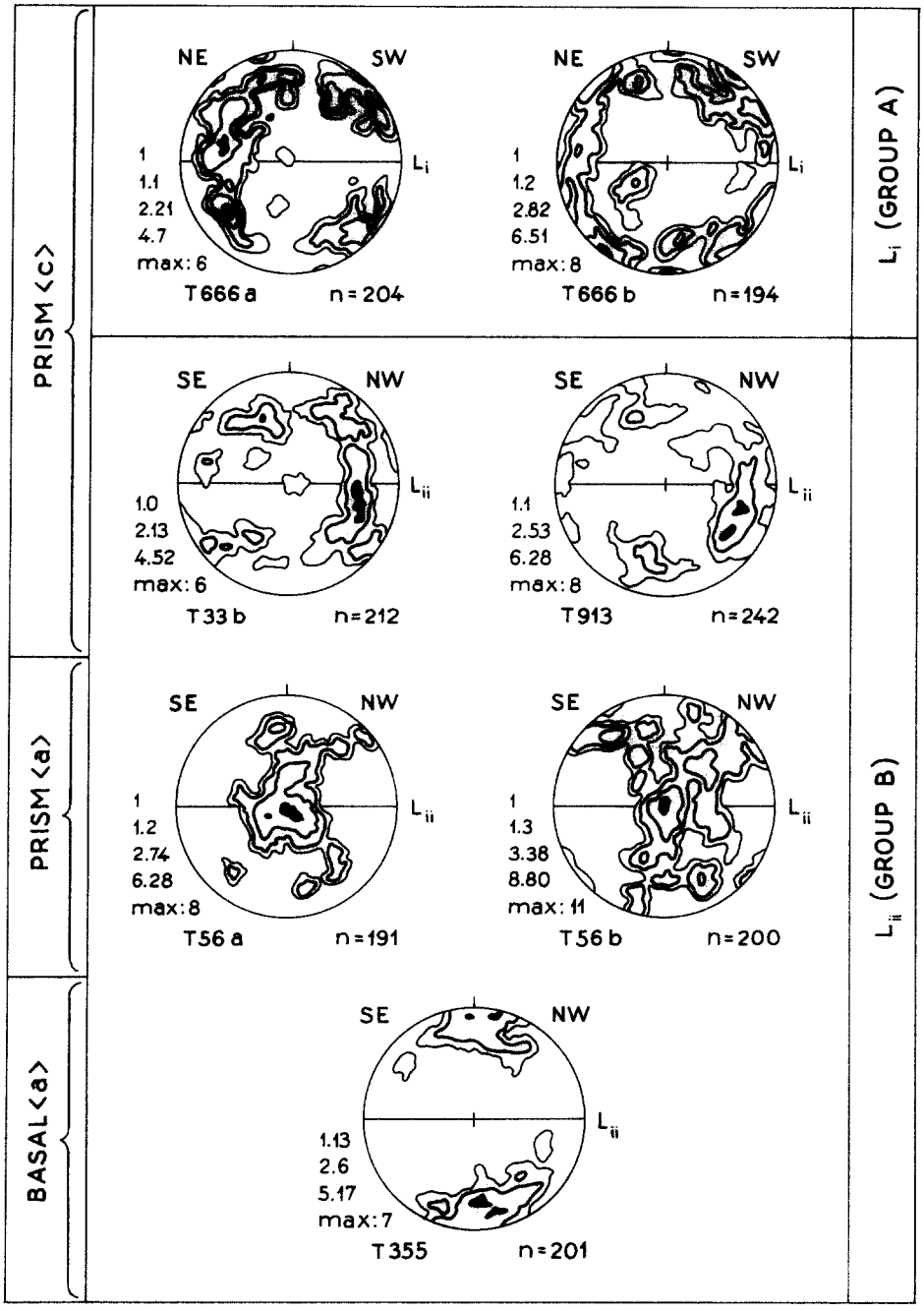

Fig. 6. Quartz *c*-axis patterns from the anatectic granite, orthogneissified granite and later shear zone. In anatectic granite (T666a, T666b, T33b and T913) the *c*-axes are concentrated along small circles around L_i or L_{ii} lineations with maxima close to L_i or L_{ii}. Prism ⟨*c*⟩ glide is suggested as dominant deformation mechanism. Quartz fabrics from orthogneissified granite (T56a and T56b) show typical type II crossed-girdle patterns of Lister (1977) with dominant prism ⟨*a*⟩ glide. Quartz fabric from shear zone (T355) indicating dominant basal ⟨*a*⟩ glide. Trace of foliation (horizontal line) and L_i or L_{ii} stretching lineations indicated. Contours and maximum density in multiples of uniform distribution.

Theoretical studies of the behaviour of linear markers embedded in deforming viscous fluids, based on Jeffery's (1922) equations (Gay 1968, Reed & Tryggvason 1974, Fernandez 1984, 1988, Freeman 1985) as well as various experimental works (Ghosh & Ramberg 1976, Fernandez 1984, 1987), have shown that markers with high length/width ratios (r) tend to behave as passive lines (March 1932).

Jeffery's (1922) equations govern the motion of an active ellipsoidal particle flowing in viscous fluid in a simple shear regime:

$$\tan\phi = r\cdot\tan[\gamma/(r+1/r)]$$
$$\tan\theta = C\cdot[\cos^2\phi + (1/r^2)\sin^2\phi]^{1/2}, \quad (3)$$

where r is the axial ratio of the particle, γ is the shear strain, θ and ϕ are the azimuth and plunge of the particle's long axis with respect to the plane of shear and C is a constant of integration. We have used equations (3) and an initially uniform distribution of 500 model markers to study the effect of the axial ratio (r) on the resulting fabric during three-dimensional simple shear. As can be seen in Fig. 10, the strength of fabric (I)

formed by markers with sufficiently high axial ratios approximates that of passive lines, whilst fabrics formed by less elongate markers are much weaker.

In populations containing markers of various axial ratios different rates of rotations of these markers produce asymmetry of the final fabric. As pointed out by Fernandez (1984), this asymmetry may theoretically be used to deduce the sense of shearing. However, because of oscillatory fabrics (Willis 1977), which appear at rather low strains for lower axial ratios (Fig. 9), an opposite asymmetry may readily appear. The use of subfabric asymmetry as an indicator of shear sense must therefore be treated with care.

To study the effect of the axial ratio of measured tourmalines on resulting fabrics we have subdivided the data from each site into two subfabrics according to their (r) value ($r = 4$ was chosen as a threshold). For all $r > 4$ and $r < 4$ subfabrics corresponding eigenvalues, eigenvectors, K and I parameters have been calculated.

According to the orientation of maximum concentration of marker axes, two principal groups of tourmaline fabrics were distinguished (Figs. 7a & b).

Group A (samples T353, T351, T666, T115)

Maximum concentration $\mathbf{v}_1$ of tourmaline axes is parallel to the NE–SW-trending L_i lineation and minimum eigenvector $\mathbf{v}_3$ is parallel to the pole of S_1 foliation. Global tourmaline fabrics lie in the flattening field or close to the $K' = 1$ line.

Group B (samples T33, T34, T32, T66, T56, T57, T701, T913a,b,c,d, T665, T335)

The eigenvectors $\mathbf{v}_1$ and $\mathbf{v}_2$ of group B fabrics also lie in the S_1 foliation plane, but $\mathbf{v}_1$ axes are parallel to the NW–SE-trending L_{ii} lineation. A switch between $\mathbf{v}_1$ and $\mathbf{v}_2$ is characteristic for the transition from group A to group B tourmaline fabrics. Various fabric types can be observed ranging from girdle distributions ($K < 1$) to constrictional clusters ($K \gg 1$).

Differences between $r > 4$ and $r < 4$ subfabrics exist in both groups A and B (Figs. 10a & b). If global fabrics are in the flattening field or close to the $K' = 1$ line, markers with higher axial ratios show in most cases more

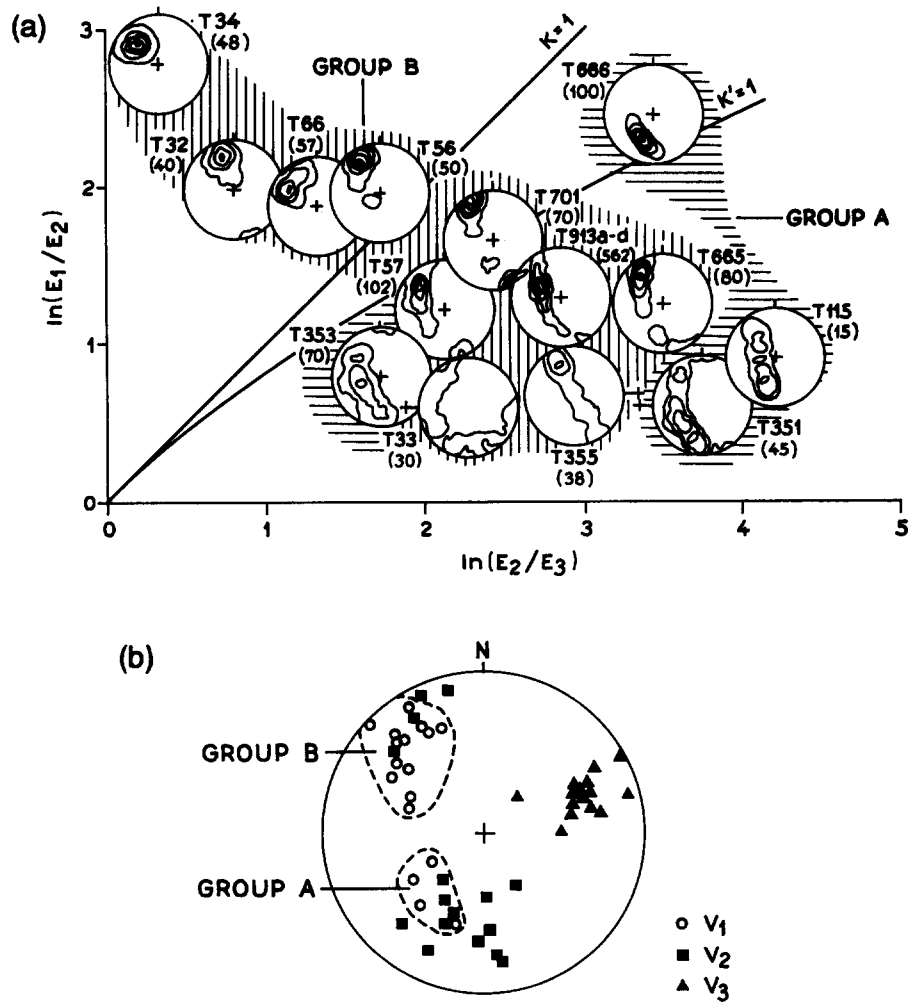

Fig. 7. (a) Woodcock's (1977) diagram showing different types of tourmaline fabrics at individual sites studied. Groups A and B are distinguished by horizontal and vertical stripes, respectively (see text for explanation). All orientation diagrams are lower-hemisphere, equal-area projections contoured at 1.2, 4.4, 7.6, 10.8, 14 multiples of uniform distribution. Numbers of tourmaline long axes measured in parenthesis. (b) Orientations of maximum ($\mathbf{v}_1$), intermediate ($\mathbf{v}_2$) and minimum ($\mathbf{v}_3$) eigenvectors deduced from individual tourmaline orientation tensors. Note the switch between $\mathbf{v}_1$ and $\mathbf{v}_2$ axes of groups A and B within the foliation plane.

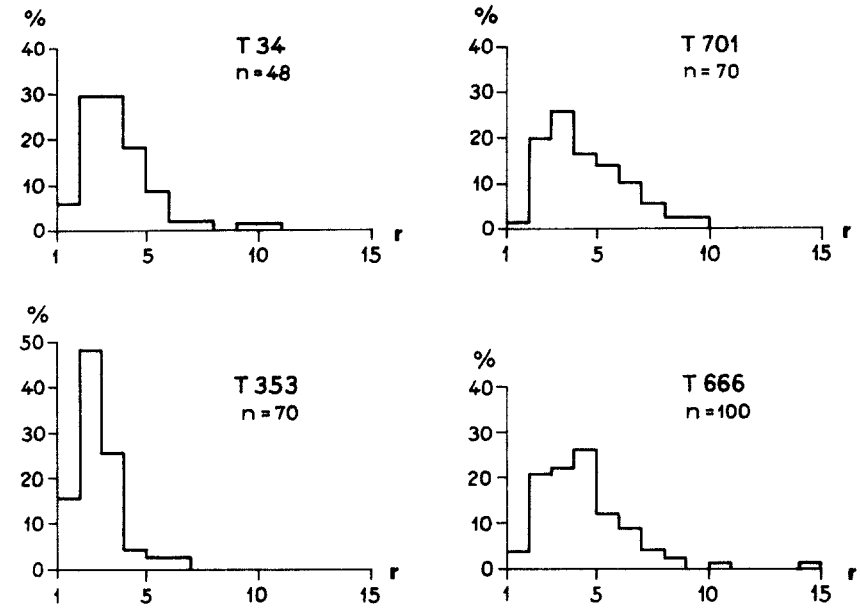

Fig. 8. Distribution histograms of tourmaline axial ratios r (length/width) of some populations measured.

intense fabrics (Figs. 11a & b and 12). This is in agreement with theoretical predictions for particle reorientation in viscous fluids. The symmetry of $r > 4$ subfabrics is often more prolate than where $r < 4$. On the other hand, in more prolate global fabrics (T34 and T56 in Fig. 10), markers with lower aspect ratio are better aligned and form more constrictional subfabrics than markers with lower axial ratio. This may be explained from field observation, since sites with intense constrictional fabrics have large tourmaline crystals which are often boudinaged, thus forming a well aligned subfabric with lower axial ratio.

NUMERICAL MODELLING

We have tried to develop a mathematical model of fabric evolution to explain the observed tourmaline fabrics. As the final fabrics (Fig. 7a) could result from an infinite number of deformation paths, we have considered several common deformations to visualize which of them could most probably produce observed fabrics.

First, an initially uniform distribution of 500 unit vectors was generated, following Sanderson & Meneilly (1981). This distribution represents the initial fabric before deformation (I in Fig. 12). Eigenvalues calculated from this distribution show negligible deviation from one another (less than 0.1%) and the number of 500 vector used for the modelling gives results with reasonable precision (Harvey & Laxton 1980).

Various types of deformation were applied to the generated uniform distribution to see which produced fabrics comparable to that observed at our localities. The orientation tensor was calculated from the deformed distribution and its eigenvalues E_1, E_2, E_3 and eigenvectors $\mathbf{v}_1$, $\mathbf{v}_2$, $\mathbf{v}_3$ used to specify the shape and orientation of final fabric.

We have assumed in our modelling, that the markers behave as passive material lines during deformation (March 1932). Because some of the tourmalines measured have low aspect ratio (r) (Fig. 8), their behaviour cannot be considered as perfectly passive (Fig. 9). This means that the strength of the model fabrics is slightly overestimated for a given amount of deformation.

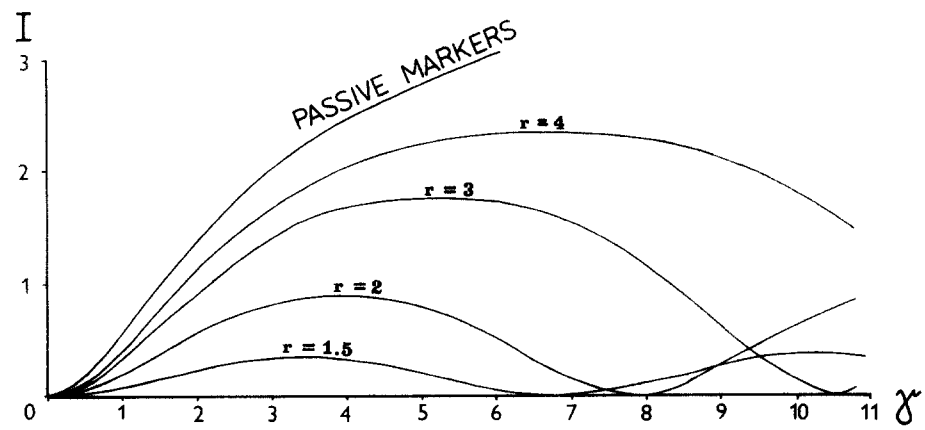

Fig. 9. Fabric strength I of initially uniform distribution of axial markers with axial ratio r deformed in simple shear regime. γ—shear strain.

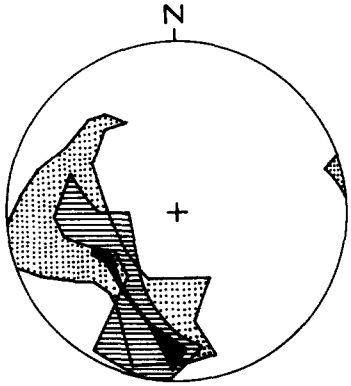

Fig. 10. Lower-hemisphere, equal-area projection of the orientation of long axes of tourmaline columns at site T-353. Three areas on the diagram are distinguished according to different aspect ratio values, r, of the tourmalines: black, $r > 4$; striped, $3 < r < 4$; dotted, $r < 3$. Note clear dependance of fabric strength on axial ratio r of the markers. $n = 70$.

Although quartz microstructures and microfabrics indicate high temperatures close to the granite solidus prevailing during both L_i and L_{ii} formation, it is not clear if these lineations originated simultaneously or if they result from superposed deformations. That is why we have considered both possibilities: (1) the simultaneous origin of perpendicular linear fabrics in a transpressive regime and (2) superposition of two different deformation phases with mutually perpendicular extension directions.

Transpression

Transpression (Harland 1971, Sanderson & Marchini 1984) is defined as a wrench shear accompanied by shortening or extension across the shear plane. Sanderson & Marchini (1984) modelled the strain variations and deformation paths in transpression. They showed that the shapes of the finite strain ellipsoid varied strongly with the amount of shortening (extension) across the shear zone, and that 'switches' between principal strain axes may occur producing lineation perpendicular to the shear direction (Sanderson & Marchini 1984, fig. 2).

Using our model we have studied the variations in fabric evolution in the transpression regime. Transpression was defined as:

$$\begin{pmatrix} 1 & 0 & \gamma \\ 0 & 1 & 0 \\ 0 & 0 & 1 \end{pmatrix} \times \begin{pmatrix} 1 & 0 & 0 \\ 0 & \alpha & 0 \\ 0 & 0 & \alpha^{-1} \end{pmatrix} = \begin{pmatrix} 1 & 0 & \alpha^{-1}\gamma \\ 0 & \alpha & 0 \\ 0 & 0 & \alpha^{-1} \end{pmatrix}, \quad (4)$$

where γ represents the shear strain and α^{-1} the shortening ($\alpha^{-1} < 1$) or extension ($\alpha^{-1} > 1$) across the zone (Fig. 12). Using different values of γ and α^{-1} we can calculate the corresponding fabric and thus study how the variation in these parameters is reflected in the resulting fabrics. Figure 12 shows the fabrics modelled for different values of γ and α^{-1}. For easy comparison between model and natural tourmaline fabrics, the modelled transpression fabrics are shown in lower-hemisphere equal-area projections (1–6 in Fig. 12) with the orientation of x-, y- and z-axes rotated to positions corresponding to that observed in the area studied (II in Fig. 12). The fabric shapes vary with α^{-1} as follows:

—simple shear deformation ($\alpha^{-1} = 1$) produces slightly oblate fabrics with $K' = 1$ symmetry (2 in Fig. 12);

—transpression ($\alpha^{-1} < 1$) results in oblate fabrics ($K' < 1$), at lower α^{-1} values ($\alpha^{-1} \ll 1$) a switch between $\mathbf{v}_1$ and $\mathbf{v}_2$ occurs so that fabrics perpendicular to the shear direction are produced (4–6 in Fig. 12) with $K' \leq 1$ symmetry;

—transtension ($\alpha^{-1} > 1$) leads to prolate fabrics ($K' \gg 1$; 1 in Fig. 12). A switch between $\mathbf{v}_2$ and $\mathbf{v}_3$ occurs at high α^{-1} values producing foliation perpendicular to the shear plane and parallel to the shear direction.

When we compare the fabrics modelled (1–6 in Fig. 12) with the tourmaline fabrics observed in our localities

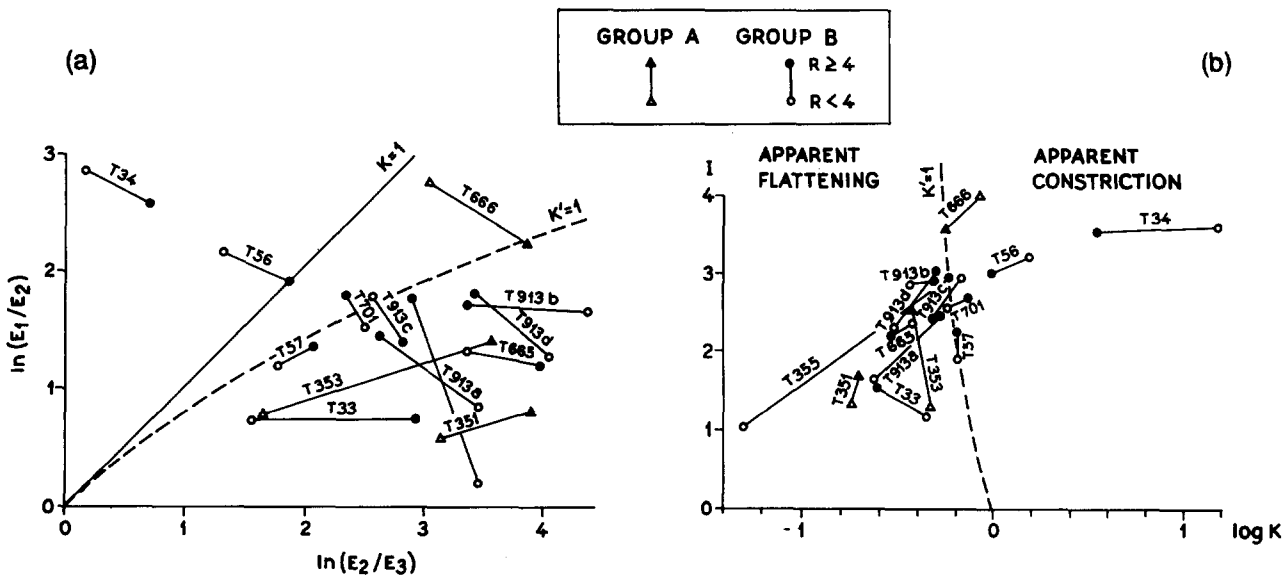

Fig. 11. (a) Woodcock's (1977) plot showing the difference between $r > 4$ and $r < 4$ tourmaline subfabrics for individual populations measured. (b) Graph of fabric intensity (I) vs fabric shape (log K) showing the differences between $r > 4$ and $r < 4$ tourmaline subfabrics. $K = \ln(E_1/E_2)/\ln(E_2/E_3)$.

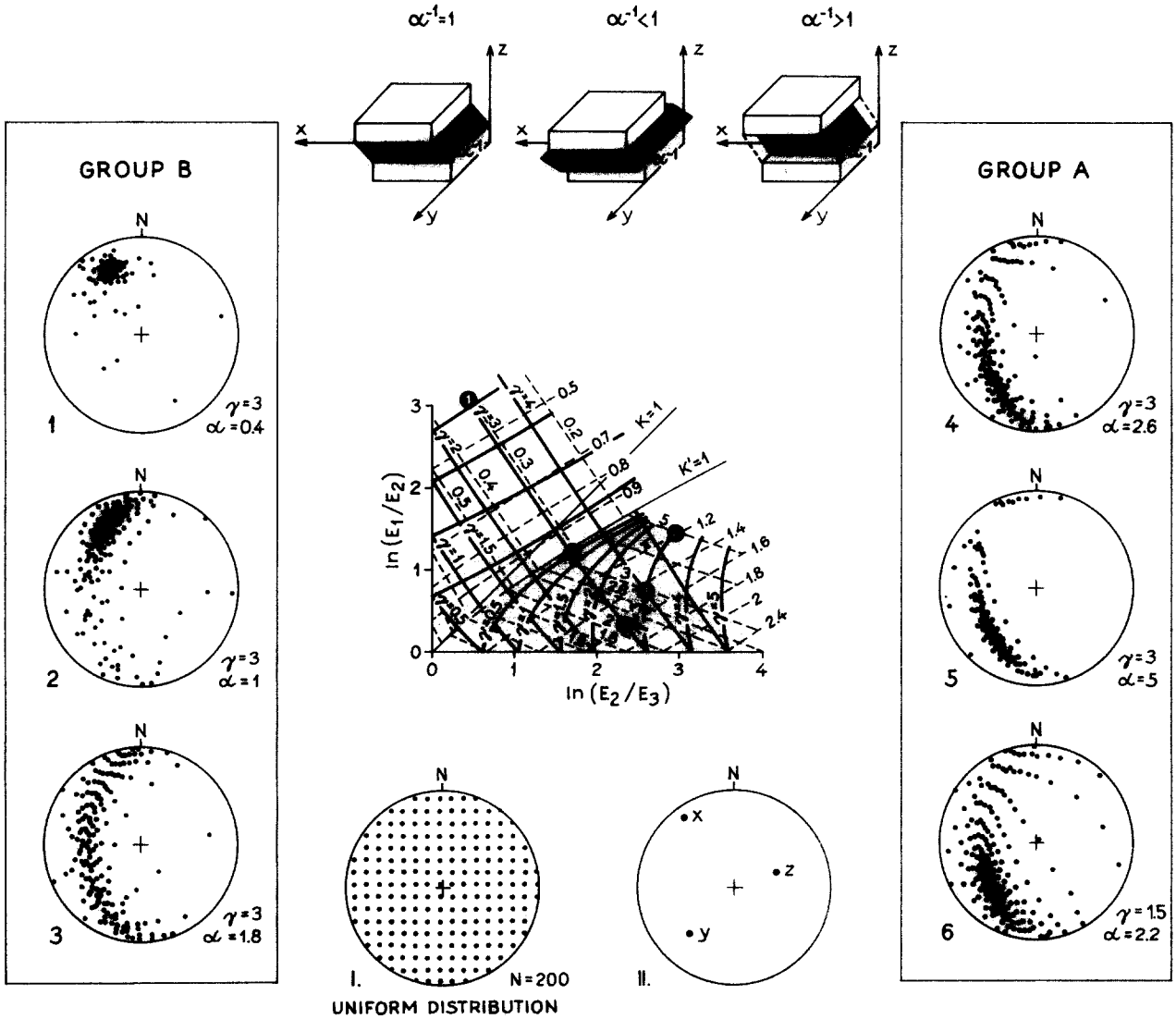

Fig. 12. Fabric modelling in transpression regime. Initially uniform distribution of passive linear markers (I) was deformed in transpression regime (see text) with x-, y- and z-axes rotated to their geographical positions in the area studied (II). Different fabric types (1–6) produced for varying α and γ parameters are shown as lower-hemisphere projections and in Woodcock's (1977) plot.

(Fig. 7a) they are very similar for shear strains, γ varying between 2 and 5, and for shortening across the zone, α varying between 0.5 and 5.

We have also modelled the development of fabrics during progressive deformation by the successive application of small increments of deformation ($\alpha_i^{-1} < 0.05$, $\gamma_i < 0.95$). The parameter T_i of Sanderson & Marchini (1984)

$$T_i = \gamma_i(1 - \alpha_i^{-1})^{-1} \quad (5)$$

was used to specify the deformation (Fig. 13).

Superposed deformations

Observed perpendicular linear fabrics could also result from two superposed deformation phases with perpendicular stretching directions. Microstructural arguments indicate that both L_i and L_{ii} lineations show signs of high-temperature origin close to granite solidus and that a decrease in temperature is associated with the L_{ii} lineation. Taking this into account, as well as other constraints of mesoscopic fabrics, e.g. shapes and intensities of tourmaline fabrics, the following two-stage evolution can be proposed:

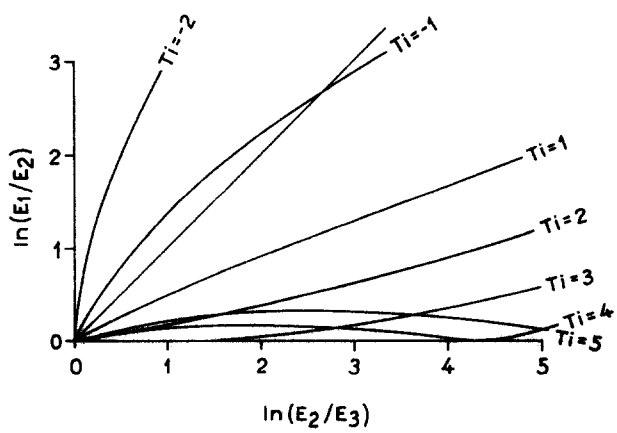

Fig. 13. Fabric paths in transpression regime shown in Woodcock's (1977) plot. Parameter $T_i = \gamma_i(1 - \alpha_i^{-1})^{-1}$ (Sanderson & Marchini 1984) specifies the deformation. See text for explanation.

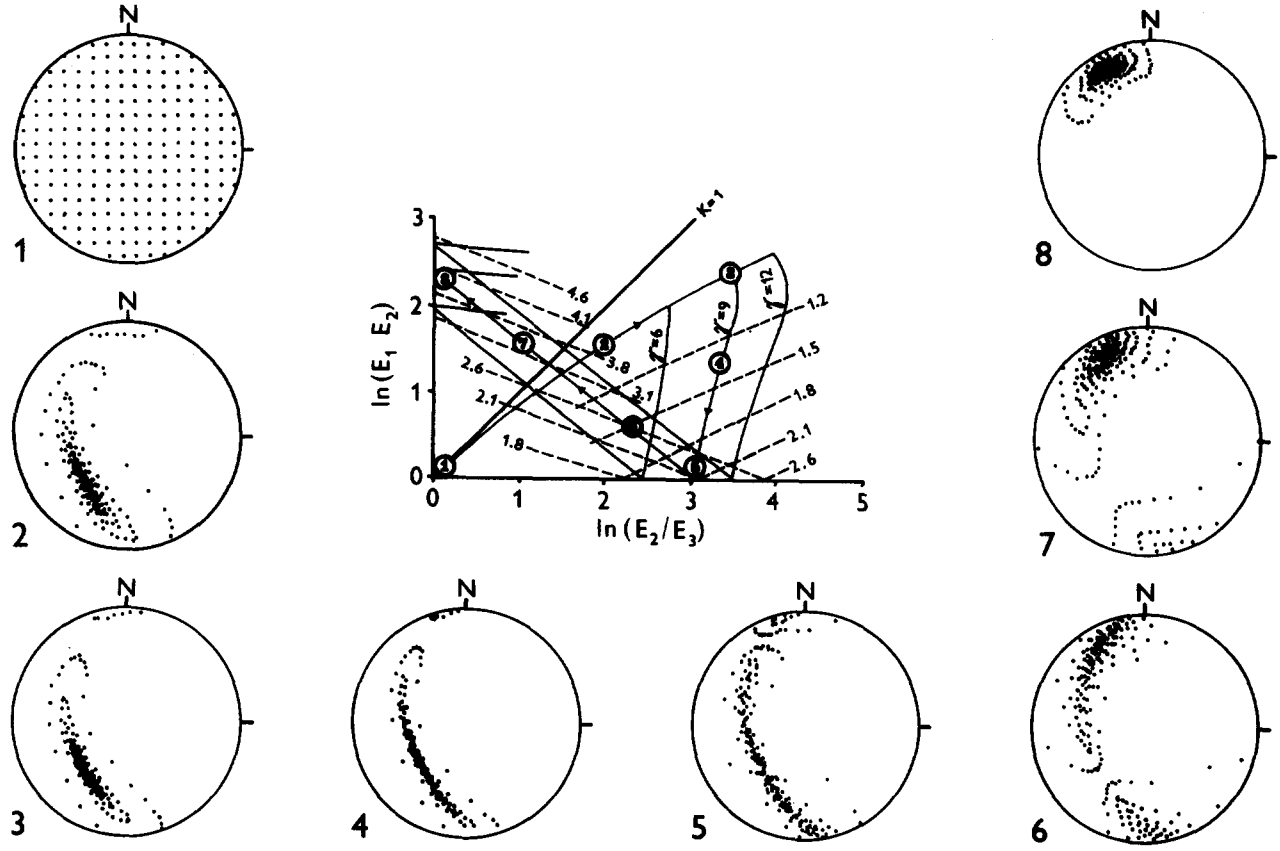

Fig. 14. Modelling of fabric evolution during two-stage deformation history. D_1 plane-strain deformation produces fabrics with SW-plunging L_i lineation (path 1–2–3) and $K' = 1$ symmetry. D_2 deformation coaxially superposed on D_1 fabrics and characterized by NW–SE subhorizontal extension, perpendicular to D_1 stretching first produces oblate fabrics (3–4–5), then switches in orientation of the longest axis of the fabric ellipsoid occurs, general triaxial fabrics (6–7) with NW-trending L_{ii} lineation and finally pure constrictional fabrics (7–8) result. See text for discussion.

(1) D_1 deformation close to magmatic–solid-state transition producing SW-plunging L_i lineations and associated group A tourmaline fabrics with $K' = 1$ symmetry;

(2) D_2 phase characterized by a switch in the orientation of the X- and Y-axes of finite strain ($X_2 = Y_1$) still under high-temperature conditions, producing a wide range of NW-trending L_{ii} linear fabrics. The final stages of D_2 occurred under lower temperature conditions.

Using a trial-and-error method, we have examined superposition of common deformations which might produce the observed fabrics. Reasonable coincidence between model and natural tourmaline fabrics was obtained for the two following strains:

D_1—plane strain deformation with X_1 extension in the SW–NE direction producing L_i lineation and X_1Y_1 foliation (1–3 in Fig. 14);

D_2—strain characterized by extension in original Y_1-axis ($X_2 = Y_1$) producing NW–SE-trending L_{ii} lineation. During the first increments of D_2 superposed on D_1, oblate fabrics are obtained (3–5 in Fig. 14) and a switch between the X- and Y-axes occurs (5 in Fig. 14). Continuing D_2 deformation produces L_{ii} linear fabrics (group B) perpendicular to D_1 extension. To follow the 5–6–7–8 path in Fig. 14, the D_2 deformation must be characterized by a constant X_2/Y_2 ratio, i.e. it must hold:

$$e_{X_2} = e_{Y_2} \geq 1; \qquad e_{Z_2} \leq 1, \tag{6}$$

where $X_2 = Y_1$, $Y_2 = Z_1$ and $Z_2 = X_1$. Three such types of deformation may exist:

(1) isovolumic deformation ($e_{X_2} = e_{Y_2} > 1$; $e_{Z_2} \ll 1$), where extension in X_2 and Y_2 is compensated by shortening in Z_2;

(2) volume decrease ($e_{X_2} = e_{Y_2} = 1$; $e_{Z_2} < 1$) with shortening in Z_2 and no change in X_2 and Y_2;

(3) volume increase ($e_{X_2} = e_{Y_2} > 1$; $e_{Z_2} = 1$) with extension in both X_2 and Y_2 and no shortening in Z_2.

To maintain constant volume during D_2, shortening in the original X_1 extension direction must be considered. However, unrealistically high values of this shortening are necessary to produce strongly constrictional fabrics (e.g. 90% shortening for fabric 8 in Fig. 14). The D_2 extension could also be compensated for by a volume increase and no shortening in X_1, but again very high values of volume increase are necessary to produce fabrics corresponding to the observed ones ($dV >$ 1000% for fabric 8 in Fig. 14). In fact the values of dilation and shortening necessary to produce fabrics similar to those observed for any combination of volume

increase and shortening in the X_1 direction during D_2 deformation are too high to accept this model as a realistic one. Moreover, the sheet-like character of the granitic bodies does not support the ballooning hypothesis.

DISCUSSION

Two mutually perpendicular stretching lineations have been observed on commonly oriented foliation planes in synkinematically emplaced leucocratic granite and surrounding mica schists of the Svratka Unit. One lineation is subhorizontal while the other is subparallel to the dip of the foliation planes. They are never developed together on one foliation plane, rather they occur in alternating domains. Both lineations are marked by a preferred orientation of tourmaline columns which define a wide range of fabrics. Tourmaline fabrics associated with the subhorizontal lineation range from oblate to constrictional shapes while fabrics associated with dip-parallel lineation exhibit plane strain to oblate shapes. Both lineations are associated with high-temperature fabrics in quartz with a dominant activity of hard prism ⟨*c*⟩ slip. The subhorizontal lineation shows a decrease in temperature manifested by the increasing importance of prism ⟨*a*⟩ slip and even basal ⟨*a*⟩ slip in quartz during a constant shear regime. Folds are mostly tight to isoclinal with axes strictly parallel to both lineations, axial planes being parallel to the regional foliation plane. Only those folds parallel to the subhorizontal lineation may be close to open and exhibit variable dips of axial planes.

Three different models have been used to explain the occurrence of two perpendicular stretching lineations in natural rocks:

(a) a combination of two simple shears with perpendicular shear directions and parallel shear plane (thrust-wrench model of Burg *et al.* 1987);

(b) the superposition of two independent deformational regimes (Cannat & Bouchez 1986), for example, early thrusting overprinted by later retrogressive perpendicular extension;

(c) transpression defined as a combination of wrench shear, shortening across and extension along the shear plane (Harland 1971, Sanderson & Marchini 1984).

The combination of two simple shears with orthogonal shear directions and the same shear plane produces generally stretching lineations oblique with respect to the direction of shear. Only when one shear component is much higher than the other may lineations subparallel to the shear direction result (Burg *et al.* 1987, fig. 2). The presence of transverse, oblique and longitudinal stretching lineations and more or less continuous changes in lineation trajectories in many areas supports the validity of this model. However, it is difficult to explain the perpendicular tourmaline fabrics in the Svratka Unit by the thrust-wrench model because: (1) no oblique lineations or continuous changes in lineation trends have been observed; and (2) fabric shapes observed vary from oblate to constrictional and do not correspond to plane strain symmetry resulting from a combination of two perpendicular simple shear deformations.

As has been shown by mathematical modelling, one possible way to obtain the observed range of fabric shapes is by coaxial superposition of two deformations with perpendicular extension directions: the D_1 deformation exhibiting plane strain symmetry and the D_2 deformation ($e_{X_2} = e_{Y_2} \geq 1$, $e_{Z_2} \leq 1$) characterized by a switch between principal axes ($X_2 = Y_1$, $Z_2 = X_1$). Early thrusting producing the SW–NE-trending dip-slip lineation followed by coaxial extension perpendicular to the initial shear direction could be used to explain the observed fabrics. However, there are only very few asymmetric structures associated with the L_i lineation, e.g. σ-porphyroclasts and asymmetries of the maxima in *c*-axis patterns which would indicate non-coaxial D_1 thrusting with possible top-to-the-northeast movement. Moreover, unrealistically high values of shortening in Z_2 and/or volume increase are necessary to produce constrictional D_2 fabrics similar to that observed.

The transpressional model (Harland 1971, Sanderson & Marchini 1984) corresponds well, from a geometrical point of view, to relatively steeply inclined foliation planes with two perpendicular lineations, one approximately strike-parallel and the other dip-parallel. The observed range of tourmaline fabrics fits well with fabric shapes produced in transpression and the switches of principal axes orientations occur as suggested in Sanderson & Marchini's (1984) model. Moreover, realistic strain magnitudes are sufficient to produce observed changes in fabric symmetry and in strain axes orientations.

Decreasing temperature conditions documented by retrograde microstructural evolution are consistent with the prevailing importance of the strike-slip component of the bulk strain during a long lasting shear regime. Folds with axes parallel to both lineations were probably formed at different stages of the deformation. Older folds with axial planes subparallel to the S_1 foliation are more flattened while later open folds with axes subparallel to strike-parallel lineation and with variable dip of axial planes are associated with relatively low-temperature deformational conditions and an extensional shear regime.

CONCLUSIONS

Detailed field mapping, mesostructural and microstructural observations in the granite of the Svratka Unit leads to the following conclusions.

(1) Leucocratic peraluminous granite was synkinematically emplaced during northwestward Variscan shearing. Indications of prism ⟨*c*⟩ glide operating in large quartz grains show high-temperature deformation conditions close to the granite solidus. Two perpendicular lineations, one subparallel and the other subperpendicu-

lar to the shear direction are associated with this stage of granite deformation.

(2) A transition in the operating slip system in quartz from prism ⟨c⟩ to prism ⟨a⟩ and basal ⟨a⟩ glide is associated with the decrease in temperature of deformation of the granite during continuing top-to-the-northwest movements.

(3) Tourmalines in the granite studied may be regarded as passive markers if their aspect ratio is large enough ($r > 5$). Tourmalines with lower aspect ratios form weaker subfabrics, which is in agreement with Jeffery's (1922) theory. However, this is not true at sites with strong post-solidus deformation, where tourmalines with lower aspect ratios are often boudinaged and better aligned than those with higher aspect ratios.

(4) Perpendicular linear fabrics marked by the preferred orientation of tourmaline may be explained by a transpressional model. Combination of dextral shearing with shortening across the shear plane and lengthening perpendicular to the shear direction is inferred in the granite near subsolidus conditions.

(5) Explanation of the observed perpendicular linear fabrics by coaxial superposition of two deformation phases seems less probable due to very high amounts of shortening and/or volume increase necessary to produce such fabrics. The origin of these fabrics in a thrust-wrench regime is also not probable.

Acknowledgements—Many thanks to D. J. Sanderson and two anonymous referees for careful reviews which improved significantly the original manuscript. We are grateful to J.-L. Bouchez, S. Vrána and D. Gapais for critical comments, A. Autran and P. Ledru for always stimulating discussions during field work and S. Figar for help with data collection. O. Čepek helped us with programming of some subroutines and S. Novák drew the figures.

REFERENCES

Behrmann, J. H. 1988. Crustal-scale extension in a convergent orogen: the Sterzing–Steinach mylonite zone in the Eastern Alps. *Geodinamica Acta* **2**, 63–73.

Blumenfeld, P., Mainprice, D. & Bouchez, J.-L. 1986. C-slip in quartz from subsolidus deformed granite. *Tectonophysics* **127**, 97–115.

Bouchez, J.-L., Mainprice, D. H., Trepied, L. & Doukhan, J. C. 1984. Secondary lineation in a high-T quartzite (Galicia, Spain): an explanation for an abnormal fabric. *J. Struct. Geol.* **6**, 159–165.

Brun, J. P., Burg, J. P. & Ming, Ch. G. 1985. Strain trajectories above the Main Central Thrust (Himalaya) in southern Tibet. *Nature* **313**, 388–390.

Burg, J. P., Bale, P., Brun, J. P. & Girardeau, J. 1987. Stretching lineation and transport direction in the Ibero–Armorican arc during the Siluro-Devonian collision. *Geodinamica Acta* **1**, 71–87.

Cannat, M. & Bouchez, J.-L. 1986. Lineations N–S et E–W en Vendée littorale (Massif armoricain). Episodes tangentiels successifs éohercyniens en France occidentale. *Bull. Soc. geol. Fr.* **8**, 299–310.

Cobbold, P. R. & Gapais, D. 1979. Specification of fabric shapes using an eigenvalue method. *Bull. geol. Soc. Am.* **90**, 310–312.

Fara, H. D. & Scheidegger, A. E. 1963. An eigenvalue method for the statistical evaluation of fault plane solutions of earthquakes. *Bull. seism. Soc. Am.* **53**, 811–816.

Fernandez, A. 1984. Etude théorique et expérimentale du développement de la fabrique dans les roches magmatiques. Application á l'analyse structurale des granitoides. Unpublished thesis, University of Clermont-Ferrand.

Fernandez, A. 1987. Preferred orientation developed by rigid markers in two dimensional simple shear strain: a theoretical and experimental study. *Tectonophysics* **136**, 151–158.

Fernandez, A. 1988. Strain analysis from shape preferred orientation in magmatic rocks. *Bull. geol. Inst. Univ. Uppsala* **14**, 61–67.

Flinn, D. 1962. On folding during three-dimensional progressive deformation. *J. geol. Soc. Lond.* **118**, 385–433.

Franke, W. 1989. Tectonostratigraphic units in the Variscan belt of central Europe. *Spec. Pap. geol. Soc. Am.* **230**, 67–90.

Freeman, B. 1985. The motion of rigid ellipsoidal particles in slow flows. *Tectonophysics* **113**, 163–183.

Gapais, D. & Barbarin, B. 1986. Quartz fabric transition in a cooling syntectonic granite (Hermitage massif, France). *Tectonophysics* **125**, 357–370.

Gay, N. C. 1968. The motion of rigid particles embedded in a viscous fluid during pure shear deformation of the fluid. *Tectonophysics* **5**, 81–88.

Ghosh, S. K. & Ramberg, H. 1976. Reorientation of inclusions by combination of pure shear and simple shear. *Tectonophysics* **34**, 1–70.

Harland, W. B. 1971. Tectonic transpression in Caledonian Spitsbergen. *Geol. Mag.* **108**, 27–42.

Harvey, P. K. & Laxton, R. R. 1980. The estimation of finite strain from the orientation distribution of passively deformed linear markers: eigenvalue relationship. *Tectonophysics* **70**, 285–307.

Jaroš, J. 1989. Variscan A-type subduction in Southeast part of Bohemian Massif. *28th Geol. Congr. Washington Abstr.* **2**, 118–119.

Jaroš, J. & Mísař, Z. 1986. Geologicko-strukturní charakteristika moravika svratecké klenby a přilehlé části morvaské svorové zóny. Charles University Prague.

Jeffery, G. B. 1922. The motion of ellipsoidal particles immersed in a viscous fluid. *Proc. R. Soc. Lond.* **102**, 161–179.

Kossmat, F. 1927. Gliederung des variszischen Gebirgsbaues. *Abh. sächs. geol. Landesamts* **1**, 1–39.

Lisle, R. J. 1985. The use of the orientation tensor for the description and statistical testing of fabrics. *J. Struct. Geol.* **7**, 115–117.

Lister, G. S. 1977. Discussion: crossed-girdle *c*-axes in quartzites plastically deformed by plane strain and progressive simple shear. *Tectonophysics* **39**, 51–54.

Lister, G. S. 1981. The effect of the basal-prism mechanism switch on fabric development during plastic deformation of quartzite. *J. Struct. Geol.* **3**, 67–75.

March, A. 1932. Mathemathische Theorie der Regelung nach der Korngestalt bei Affiner Deformation. *Z. Kristallogr.* **81**, 285–298.

Matte, Ph. 1986. Tectonics and plate tectonic model for the Variscan belt of Europe. *Tectonophysics* **126**, 329–374.

Mísař, Z. 1965. Vysvětlivky k listu Bystřice nad Pernštejnem. Unpublished M.S., Geofond Prague.

Molnar, P. & Tapponier, P. 1975. Cenozoic Tectonics of Asia: effects of a continental collision. *Science* **189**, 419–426.

Němec, D. 1979. Zinnbringende orthogneisse im Suden der Antiklinale von Svratka und Ihre Erzmineralisierung. *Z. Geol. Wiss.* **7**, 1437–1447.

Nicolas, A. 1984. *Principes de Tectonique*. Masson, Paris.

Pertoldová, J. 1986. Podmínky vzniku skarnu na ložiskách Pernštejn, Županovice a Nové Město p. Smrkem. Unpublished thesis, Charles University Prague.

Reed, J. L. & Tryggvason, E. 1974. Preferred orientations of rigid particles in a viscous matrix deformed by pure shear and simple shear. *Tectonophysics* **24**, 85–98.

Sanderson, D. J. & Marchini, W. R. D. 1984. Transpression. *J. Struct. Geol.* **6**, 449–458.

Sanderson, D. J. & Meneilly, A. W. 1981. Analysis of three-dimensional strain modified uniform distributions: andalusite fabrics from a granite aureole. *J. Struct. Geol.* **3**, 109–116.

Scheidegger, A. E. 1965. On the statistics of the orientation of bedding planes, grain axes and similar sedimentological data. *Prof. Pap. U.S. geol. Surv.* **525-C**, 164–167.

Schulmann, K., Ledru, P., Autran, A., Melka, R., Lardeaux, J.-M., Urban, M. & Lobkowicz, M. 1991. Evolution of nappes in the eastern margin of the Bohemian Massif: a kinematic interpretation. *Geol. Rdsch.* **80**, 73–92.

Schulmannová, B. 1987. Petrostrukturní analýza metamorfovaných hornin v okolí skarnového tělesa u Věchnova. Unpublished thesis, Charles University Prague.

Shackleton, R. M. & Ries, A. C. 1984. The relation between regionally consistent stretching lineations and plate motions. *J. Struct. Geol.* **6**, 111–117.

Suess, F. E. 1912. Die moravischen Fenster und ihre Beziehung zum Grundgebirge des Hohen Gesenke. Denkschr. *Akad. Wiss. math.-naturwiss.* **LXXXVII**, 541–631.

Suess, F. E. 1926. *Intrusions—Tektonik und Wandertektonik in Variszischen Gebirge*. Borntrager, Berlin.

Van Breemen, O., Aftalion, M., Bowes, D. R., Dudek, A., Mísař, Z., Povondra, P. & Vrána, S. 1982. Geochronological studies of the Bohemian Massif, Czechoslovakia, and their significance in the evolution of central Europe. *Trans. R. Soc. Edinb., Earth. Sci.* **73**, 89–108.

Watson, G. S. 1965. The statistics of orientation data. *J. Geol.* **74**, 786–797.

Weiss, J. 1966. Ultrabasic rocks of the West Moravian crystalline complex. *Krystalinikum* **4**, 171–184.

Willis, D. G. 1977. A kinematic model of preferred orientation. *Bull. geol. Soc. Am.* **88**, 883–894.

Woodcock, N. H. 1977. Specification of fabric shapes using an eigenvalue method. *Bull. geol. Soc. Am.* **88**, 1231–1236.